Cu-Mn-Co oxides as protective materials in SOFC technology

Masi, Andrea; Bellusci, Mariangela; McPhail, Stephen J.; Padella, Franco; Reale, Priscilla; Hong, Jong-Eun; Steinberger-Wilckens, Robert; Carlini, Maurizio

DOI:
10.1016/j.jeurceramsoc.2016.09.025

Cu-Mn-Co oxides as Protective Materials in SOFC Technology: the Effect of Chemical Composition on Mechanochemical Synthesis, Sintering Behaviour, Thermal Expansion and Electrical Conductivity

Andrea Masi 1-3, Mariangela Bellusci 1, Stephen McPhail 1, Franco Padella 1, Priscilla Reale 1, Jong-Eun Hong 2, Robert Steinberger-Wilckens 2, Maurizio Carlini 3

1) ENEA C.R. Casaccia, 00123 Rome, Italy

2) School of Chemical Engineering, University of Birmingham, Edgbaston, Birmingham B15 2TT, UK

3) University of Tuscia - DAFNE, 01100 Viterbo, Italy

Abstract

To study the effect of the composition on the physico-chemical properties of mixed Cu-Mn-Co oxides as SOFC interconnects coating materials, different compounds have been obtained through a High Energy Ball Milling (HEBM) process. The mechanochemical treatment produces highly activated multi-phase powders that easily react at intermediate temperature to form the equilibrium products. Thermogravimetric, dilatometric and in-situ high temperature analyses allowed to show that Copper addition promotes cubic spinel stability at low temperature and enhances sintering behaviour.

Dilatometric and conductivity analysis carried out on sintered pellets allowed to obtain simple relations between the materials properties and the composition. Coefficient of Thermal Expansion (CTE) and electrical conductivity are increased by Copper doping and high Co:Mn ratios. These findings suggest that the materials characteristics can be opportunely tuned through appropriate composition design, to simultaneously obtain enhanced sintering behaviour, high electrical conductivity and CTE adapted to match the substrate.

Keywords

Spinel oxides;

Ball Milling;

Thermal Expansion;

Solid Oxide Fuel Cell;

Interconnect Coating.

1. Introduction:

Solid Oxide Fuel Cells (SOFCs) represent promising energy conversion devices characterized by high efficiency and virtually absent polluting emissions. To achieve high power required for practical use, the cells are assembled in series to obtain stacks, and a crucial part for the stack design is represented by the cell interconnect. Its role is to separate cathode and anode side of adjacent cells maintaining electrical link and granting structural stability and support. Mechanical compatibility, chemical stability, gas impermeability and high electrical conductivity are needed for proper functionality.

In the last decade, research on cell materials permitted to lower operating temperatures below 800°C, allowing to design stacks with metallic interconnects characterized by reduced costs and enhanced processability with respect to traditional ceramic parts. Among the metal alloys, Cr-rich ferritic stainless steels possess the Coefficient of Thermal Expansion (CTE) compatibility with SOFC materials, and low cost requirements needed for mass production. In operating environment these alloys undergo however severe corrosion issues, resulting in significant degradation of cell performances. The growth of superficial chromium-rich oxides, besides lowering electrical conductivity, leads in fact to significant chrome volatilization and its subsequent reaction with cathode materials, lowering the cathode active area. Protective coatings that grant electrical conductivity for long term application, inhibiting Cr volatilization, are therefore required[1,2].

For this purpose, Mn-Co spinels have been suggested as best candidates, due to their high electrical conductivity and thermal expansion compatibility with ferritic alloys [3]. The composition and thermal history of these compounds influence directly the reticular structure and the chemico-physical properties of the materials [4,5], and several studies have been carried out to further tune mechanical compatibility or electrical properties. The addition of transition metals or reactive elements such as Fe, Ti, Cu, Ni or Y has been evaluated, preparing powders and coating with several methods [6–9]. In particular, it has been observed that the composition affects the thermal expansion behaviour of the compound, and several studies include dilatometric analyses on doped or undoped Mn-Co spinels [3,7,9–15]. While some indications on how chemical composition affects CTE can be deduced (with high Mn, Fe or Ti content decreasing CTE [12] or Ni and Cu increasing CTE [7,9,16]) no clear relation between dopant amount and CTE can be inferred due to significant scattering of the reported results.

In our previous work, we have evaluated High Energy Ball Milling (HEBM) as synthesis technique of mixed Mn-Co spinels starting from Mn and Co oxides [17]. HEBM is a mechanochemical technique in which the kinetic energy of colliding balls is transferred to powders trapped against the vial walls. The energy transfer, beside producing comminution and nanostructuration of the powders, promotes interdiffusion of the different chemical elements, atomic rearrangements, nucleation of new phases and other phenomena [18]. Due to the impulsive nature of the energy transfer mechanism, occurring near room temperature, the products are often characterized by metastable phases and highly reactive behaviour [19–21]. In our explorative work we observed that to complete the mechanochemical solid state reaction of Mn and Co oxides, long mechanochemical treatments are needed, but short milling times (i.e. 10 hours) are effective to obtain a highly reactive multi-phase powder. The milled powder can easily form in-situ the equilibrium products during sintering treatments. HEBM is therefore proposed as potential substitute of the high temperature solid state reaction synthesis usually exploited to produce these mixed oxides.

In this work, different Mn-Co and Cu-Mn-Co oxide mixtures have been subjected to a short HEBM treatment to prepare spinels characterized by different chemical composition. The compositions were chosen to evaluate how different Mn:Co ratios, possibly in presence of copper, can affect the materials response to the mechanochemical treatment and its properties when exposed to high temperature. High temperature phases evolution, phase stability and sintering behaviour of the treated powder have been studied by means of thermogravimetric analysis, in-situ high temperature X-Ray Diffraction (XRD) and dilatometric measurements. Also the effect of the composition on thermal expansion and electrical conductivity has been evaluated and discussed.

2. Experimental Procedure

The HEBM treatment was carried out using a SPEX8000M mixer mill, cylindrical steel vials (60 cm^3 volume) and steel balls (10mm diameter) for 10 hours. Stoichiometric amounts of Mn_3O_4 (Sigma Aldrich, 97%), Co_3O_4 (Sigma Aldrich, 99%) and CuO (Carlo Erba, 99%) were mixed in order to obtain the samples with composition reported in Table 1. A powder to balls weight ratio of 1:10 was used for the experiments; vials were loaded with 8g of powders and sealed under argon atmosphere.

Table 1: Sample nomenclature and nominal composition:

Sample name	Metal ratio			Corresponding composition
	Mn	Co	Cu	
MnCo2	0.33	0.67		$MnCo_2O_4$
Mn1.25Co1.75	0.42	0.58		$Mn_{1.25}Co_{1.75}O_4$
Mn1.5Co1.5	0.50	0.50		$Mn_{1.5}Co_{1.5}O_4$
Mn1.33Co1.17Cu0.5	0.44	0.39	0.17	$Mn_{1.33}Co_{1.17}Cu_{0.5}O_4$
Mn1.58Co0.93Cu0.5	0.52	0.31	0.17	$Mn_{1.57}Co_{0.93}Cu_{0.5}O_4$
Mn2.05Co0.45Cu0.5	0.68	0.15	0.17	$Mn_{2.05}Co_{0.45}Cu_{0.5}O_4$

A 120° angular dispersion X-ray diffractometer (XRD3000 from Italstructure, curved PSD detector from INEL), equipped with Fe $K_{\alpha1}$ radiation source, was used to perform X-Ray diffraction analysis (XRD). Phase identification was performed on collected patterns using the PDF-2 database[22] as reference data. Lorentzian fitting of selected reflections allowed to evaluate cell parameters and to calculate accordingly theoretical densities, considering nominal compositions of the samples. In situ high temperature measurements were performed installing a heating reactive chamber (Anton Paar

Gmbh, Graz, Austria). The measurements were carried out in air, at heating and cooling rates of 10°C/min, 300 s of thermal equilibrium time before the measurements and 300 s of acquisition time.

Scanning Electron Mycroscophy (SEM) analyses were carried out on a Hitachi TM3030Plus SEM equipped with EDX energy-dispersive X-ray (EDX) microanalysis.

N_2 adsorption at 77K technique (Quantachrome Autosorb-iQ) was exploited to evaluate mean particle size. Specific Surface Area (SSA) was calculated applying the BET method[23]. Average particle size was calculated assuming spherical particle shape.

Thermogravimetric analyses were carried out in air using a Pyris Diamond TG/DTA (Perkin Elmer), heating the samples up to 1200°C at 5°C/min, followed by 60 minutes of high temperature dwell time and cooling to room temperature at 5°C/min.

Dilatometric measurements were carried out using a push-rod dilatometer (DIL 402 C, NETZSCH). To evaluate sintering behaviour, consolidated pellets of about 6mm diameter were obtained by uniaxial cold pressing (3.5 T/cm^2). The experiments were carried out heating at 5°C/min scan rate up to 1200°C. To measure thermal expansion, experiments were carried out on pellets of about 6mm diameter and 2.5mm height sintered as described later in the text. The measurements were carried out with a heating rate of 10°C/min. Average CTE was calculated between room temperature and 800°C as: $CTE = \frac{1}{L_0}\frac{\Delta L}{\Delta T}$, where L_0 represents the initial length and ΔL the length change occurring in the ΔT temperature range.

Electrical conductivity was estimated by applying the Van der Pauw method [24] on pellets of about 10mm diameter, obtained by uniaxial cold pressing (3.5 T/cm2) and successive sintering (see below for experimental details). The 500-800°C temperature range was investigated, using a PAR273A potentiostat coupled to a HP 3457A multimeter. Activation energy E_a was calculated from the Arrhenius plot obtained using the formula: $\sigma = \frac{\sigma_0}{T} e^{-\frac{E_a}{kT}}$, with σ electrical conductivity, T temperature, σ_0 pre-exponential factor, E_a activation energy and k Boltzmann's constant.

3. Results and discussion

3.1. Powder characterization

The mechanochemical treatment produces fine black powders. After the milling treatments, EDX analyses have been successfully carried out to exclude the presence of iron and chromium that could highlight chemical contamination from the milling equipment. In Fig. 1 are reported the XRD patterns of the samples after 10 hours of milling. Significant peak broadening can be observed due to nanostructuration of diffractive domains and lattice defectivity induced by the HEBM treatment. The three Mn-Co samples evidence the residual presence of the Co_3O_4 precursor phase (JCPDS card n. 42-1467). The observed asymmetry towards lower angles can be related to the nucleation of a mixed $MnCo_2O_4$ phase (JCPDS card n. 23-1237). Only the Mn1.5Co1.5 sample shows signals related to the Mn_3O_4 precursor phase (JCPDS card n. 24-0734).

Cu-containing samples show similar peak broadening. The Mn1.33Co1.17Cu0.5 pattern exhibits mainly reflections compatible with the Co_3O_4 phase, with the already observed asymmetry towards lower angles. Small broadened peaks at $2\theta \cong 45$ and $2\theta \cong 49$ degrees are ascribable to the presence of CuO phase (JCPDS card n. 48-1548). Raising Mn content, reflections related to Mn_3O_4 become evident, similarly to what was observed for the Mn-Co samples.

The higher stability exhibited by the cobalt precursor phase in comparison with to the Mn and Cu oxides with respect the mechanochemical action is clearly evident from these results. The Mn1.5Co1.5 sample, composed by similar Co and Mn amounts, is characterized by Mn_3O_4 reflections scarcely visible with respect to the cubic Co_3O_4 phase peaks. Regarding copper oxide, it can be clearly observed from the pattern related to the Mn2.05Co0.45Cu0.5 sample, that also the CuO phase gets easily destructured during the milling, the CuO peaks being significantly lower and broader with respect to those of cobalt oxide. The observed phenomena can be ascribed to the difference in hardness of the materials, with Co spinel characterized by significantly higher hardness with respect to Haussmannite (Mohs hardness: 5.5) [25] and Tenorite (Mohs hardness:

3.5-4). The successive destructuration of the crystalline phases easily promotes interdiffusion of Mn and Cu atoms in the Co precursors phase or in the nucleating mixed spinel lattice.

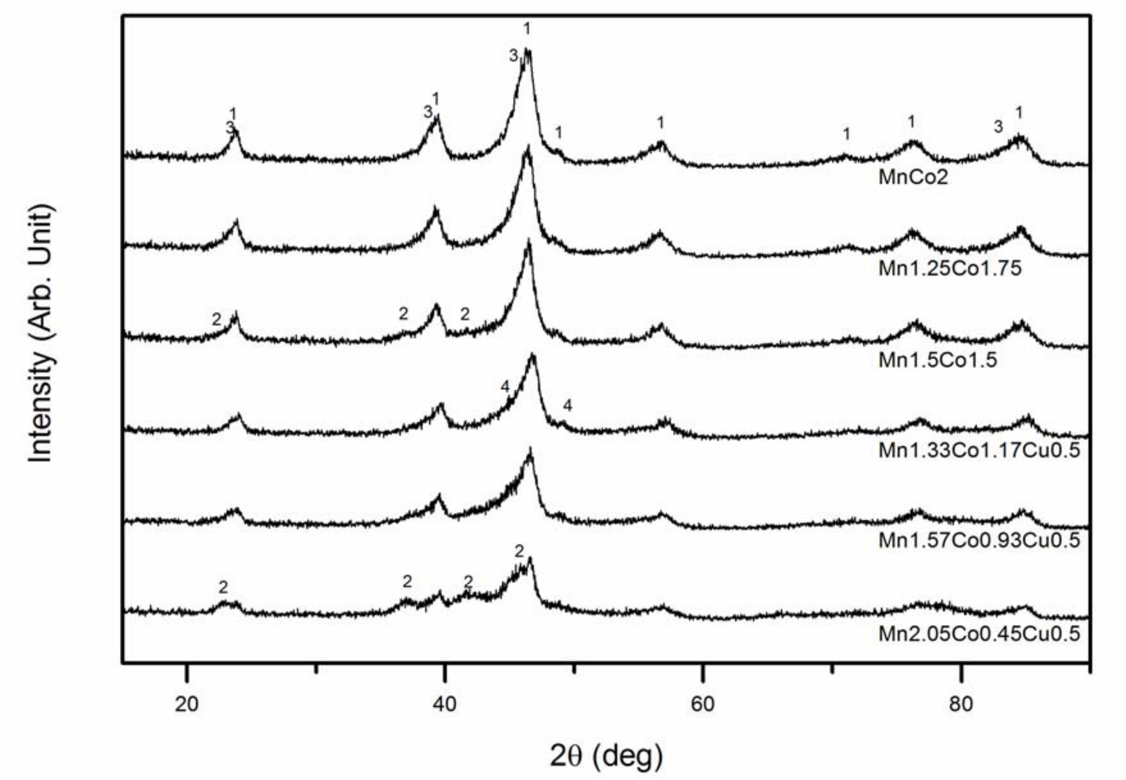

Fig. 1. X-ray powder diffraction patterns of the different samples after 10h of milling; 1) Co_3O_4 2) Mn_3O_4) $MnCo_2O_4$ 4) CuO reflections.

In Table 2 BET specific surface area and calculated mean particle size are reported. All the samples exhibit comparable values, with Copper-containing powders characterized by the lower BET area, suggesting that Copper addition promotes higher aggregation degree. Mean particle size ranges between 170 and 330nm.

Table 2: BET surface area and BET particle size for the 10h HEBM powders:

Sample	BET	l*

	(m^2/g)	(nm)
MnCo2	6.2±0.3	176±9
Mn1.25Co1.75	5.7±0.3	195±10
Mn1.5Co1.5	4.5±0.2	255±12
Mn1.33Co1.17Cu0.5	4.2±0.2	265±13
Mn1.57Co0.93Cu0.5	3.5±0.2	325±15
Mn2.05Co0.45Cu0.5	4.1±0.2	293±13

$*\boldsymbol{l} = \frac{6}{A_{BET} \cdot \rho}$

In order to evaluate how the different Mn:Co ratios and the Cu addition influence the high temperature properties of the samples, the milled powders were subjected to thermogravimetric analysis. In Fig. 2 thermogravimetric analysis curves are reported. All samples show a weight loss step ascribable to the departure of adsorbed humidity. In the 200-500°C temperature range, a gradual weight increase can be observed for all compositions. The effectiveness of mechanochemical activation can be recognized from this phenomenon: the HEBM treatment promotes in fact high degree of interdiffusion of the starting oxides, and being carried out in Ar atmosphere it is likely to create anion defective lattices. The highly defective and nanostructured powders will easily react at low temperature with oxygen, most likely leading to the oxidation of Mn to higher oxidation states. The low cation mobility at low temperature does not however allow major lattice rearrangement, producing metastable non-stoichiometric compounds. Similar metastable mixed valence spinels have been already observed for transition metal oxide systems, although prepared by other routes, and their formation was related to a high reactivity associated with highly nanostructured compounds [26].

Raising the temperature, in the 500-700°C temperature range, the Mn-Co and Mn1.33Co1.17Cu0.5 samples show a similar gradual weight loss, reaching a plateau for higher temperatures. In this temperature range, for the Mn-Co samples the reaction between the activated precursors is expected

[17]. The release of the extra oxygen content acquired during the previous weight acquisition step, followed by an interval of weight stability, is compatible therefore with the reorganization of the metastable oxidized lattices to form high temperature stable phases.

The Mn richest samples, i.e. Mn1.57Co0.93Cu0.5 and Mn2.05Co0.45Cu0.5, undergo instead a further weight acquisition step before exhibiting weight loss. In our previous work we had observed how the presence of Mn-rich unreacted spinels could lead to the oxidation of $Mn_3O_4$to Mn_2O_3 during heating, and it is likely to ascribe this weight gain to a similar phenomenon. Raising further the temperature, the oxidized compound reacts with the existing spinels, resulting in weight loss and formation of spinel phases. The behaviour of the Cu-doped samples will be further investigated in the next section by means of the outcome of in-situ high temperature XRD analysis.

Further heating over 1000°C leads to an additional weight loss phenomenon for all samples except Mn1.5Co1.5. Regarding Mn-Co samples, it is known that at high temperature, a multi-phase boundary between spinels and reduced Me^{II} oxide phases exists for Co-Mn oxide mixtures [4], with equilibrium temperature increasing with Mn content. The absence of the weight loss phenomena for the sample Mn1.5Co1.5 indicates for this composition a phase boundary temperature beyond 1200°C. In the case of Cu addition, a similar behaviour can be supposed, with a dual phase region also for the mixed Cu-Mn-Co oxides. Unlike Mn-Co samples, the weight loss is observed for all the compositions. Considering that the Mn2.05Co0.45Cu0.5 sample is characterized by an approximate 4:1 Mn:Co ratio, it is evident that copper lowers significantly the dual phase region boundary temperature.

During cooling, the high temperature weight loss phenomenon is recovered for all samples, and no significative weight change phenomena can be observed.

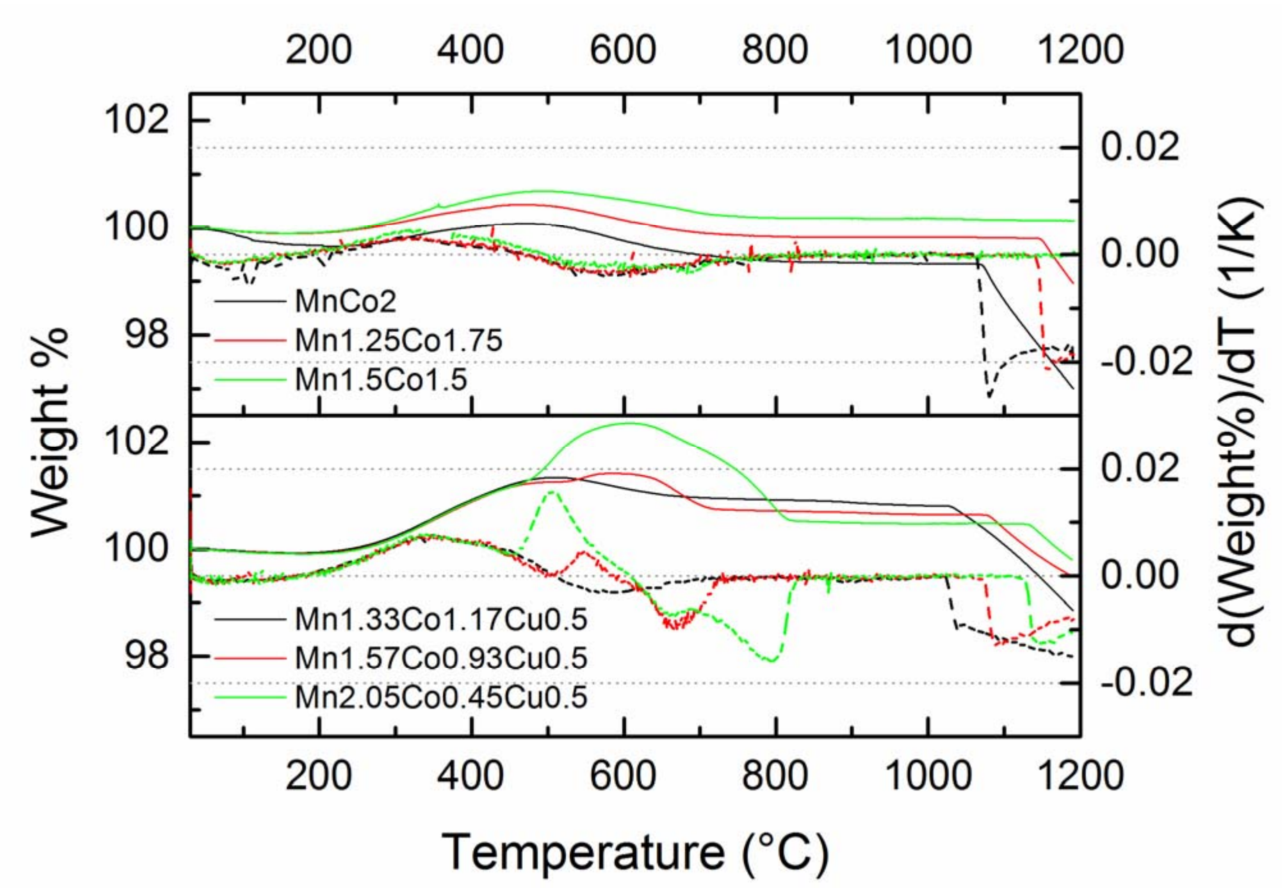

Fig. 2. Thermogravimetric curves as a function of temperature for the different samples; solid lines represent weight% change, dotted lines the derivative.

To further investigate the behaviour of the Cu doped samples upon heating, in situ diffraction analyses were carried out on the ball-milled powders. High temperature patterns are reported in Fig. 3.

Starting from the Mn1.33Co1.17Cu0.5 sample, the pattern collected at 400°C is substantially similar to that acquired at room temperature, confirming that the oxidation phenomena observed with TGA measurements do not involve reactions or significant nucleation of new phases. The reaction between the activated precursors is instead evident at 500°C, where the nucleation of a cubic spinel phase occurs. Heating further, the reaction between the remaining precursors carries on, forming a single cubic spinel phase. The weight loss observed in the 500-700°C by thermogravimetric measurements can be associated therefore to the rearrangement of the metastable oxidized lattice, resulting in the nucleation of the high temperature spinel. During cooling, no structural changes are evident, showing that the examined composition is characterized by a single phase nature in the ambient – 800°C temperature range.

The initial evolution of Mn1.57Co0.93Cu0.5 sample is similar, with the nucleation of a cubic spinel phase in the 400°C-500°C interval. At 600°C reflections ascribable to the Mn_2O_3 phase (JCPDS card n. 24-0508) are visible, explaining the thermogravimetric weight gain occurring in the 600-700°C range. The growth of the spinel phase carries along with it the increase of peaks related to this Mn-rich phase up to 700°C. Between 700°C and 800°C the rising spinel phase and Mn_2O_3 react, and the pattern collected at 800°C is ascribable to the presence of a single spinel phase. During cooling, this phase is stable down to 500°C. At 400°C, reflections ascribable to a tetragonal spinel phase similar to Mn_2CoO_4 (JCPDS 48-1548) appear, indicating the decomposition of the high temperature cubic phase with the formation of a dual phase compound.

Regarding the Mn2.05Co0.45Cu0.5 sample, coherently with thermogravimetric results, nucleation of large amounts of the oxidized Mn_2O_3 phase occur already at 500°C, along with the formation of a cubic spinel phase. The transformation of Mn_3O_4 and Co_3O_4 precursor phases occurs between 500°C and 700°C, where only Mn_2O_3 and the spinel phase are visible. Raising the temperature, Mn_2O_3 and the spinel phase react, and at 800°C the spinel phase formation is almost complete. Similarly to what was observed for the Mn1.57Co0.93Cu0.5 sample, during cooling the segregation of a tetragonal spinel phase is observed at a temperature value between 700°C and 600°C.

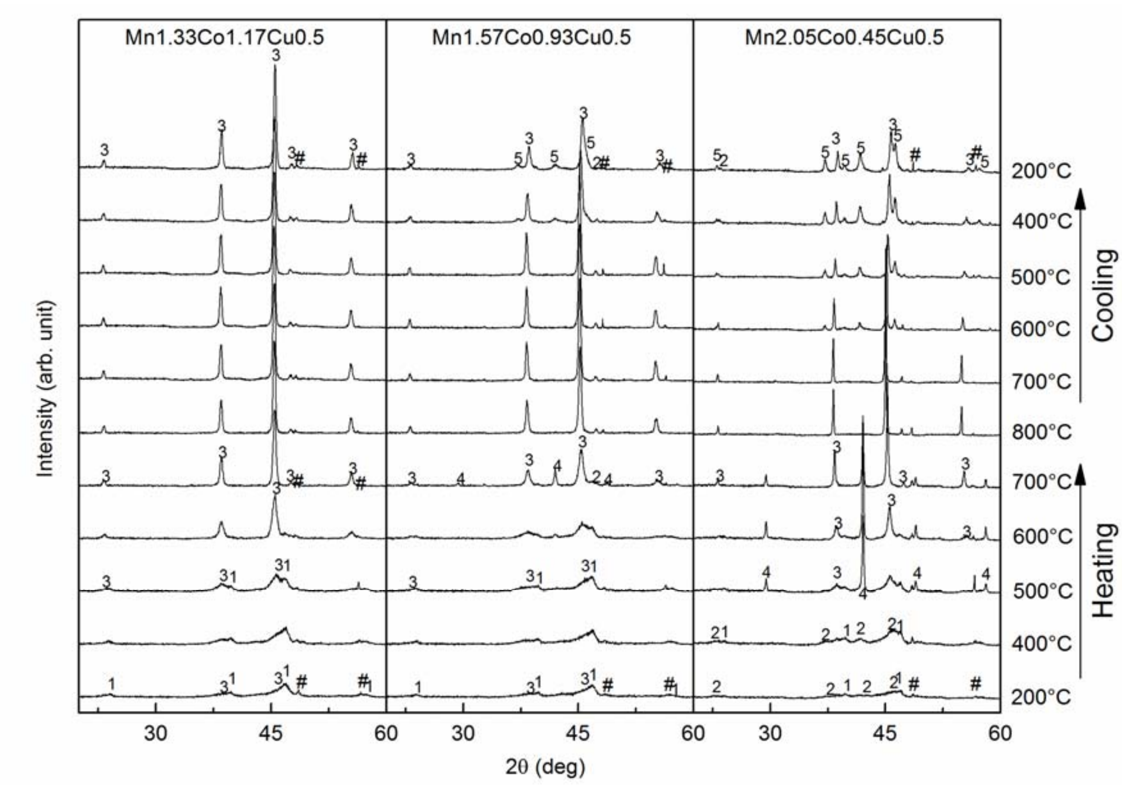

Fig. 3: In situ X-ray diffraction patterns of a) Mn1.33Co1.17Cu0.5, b) Mn1.57Co0.93Cu0.5 and c) Mn2.05Co0.45Cu0.5 samples milled for 10 hours collected at different temperatures (heating rate = 10°C/min). Reflections ascribable to 1) Co_3O_4 2) Mn_3O_4 3) $MnCo_2O_4$ 4) Mn_2O_3 5) Tetragonal mixed spinel phase and #) sample holder are indicated.

The evaluation of sintering behaviour was carried out on consolidated pellets prepared by uniaxial cold pressing. To compare sintering properties meaningfully, and ascribe differences to chemistry rather than to morphology of the powders, comparable pellet density is crucial. The geometric green densities are reported in Table 3: similar values are obtained for all the different samples, as expected from the processing of morphologically similar powders. The consolidated pellets were subjected to dilatometric measurements between room temperature and 1200°C, with a 5°C/min heating rate. Shrinkage curves are reported in Fig. 4. No significant differences can be observed between Mn-Co samples, with sintering temperatures of about 1040-1060°C and maximum densification rates at approximately 1150°C. Copper addition greatly enhances sintering behaviour: sintering temperatures are lowered to about 910°C, 870°C and 830°C respectively for

Mn1.33Co1.17Cu0.5, Mn1.57Co0.93Cu0.5 and Mn2.05Co0.45Cu0.5, and the shrinkage extent is greatly increased with respect to Mn-Co samples. High temperature dilatation phenomena are however visible in Mn1.33Co1.17Cu0.5 and Mn1.57Co0.93Cu0.5 curves. To further investigate this phenomenon, a pellet obtained by pressing Mn1.33Co1.17Cu0.5 powder was heated in furnace at 1200°C for 10 minutes and slowly cooled. The SEM image is reported in Fig. 5a. Significant grain growth and inter-grain porosity can be observed, as well as the presence of an irregular and corrugated Cu-rich phase. The observation of the samples clearly suggests a liquid phase sintering at high temperature, most likely due to segregation and melting of the Cu-rich phase, that could result in swelling phenomena [27]. The contemporary release of oxygen gas, as observed by thermogravimetric analysis, when occurring in a highly packed structure could furthermore enhance the expansion phenomena.

XRD analysis of the pellets after dilatometric measurements demonstrated in most cases secondary phases in addition to the spinel. Differently from TGA measurements, the pelletized materials did not recover the oxygen loss properly during cooling, probably due to higher packing of particles, high crystal growth and subsequent reduced oxygen diffusion kinetics.

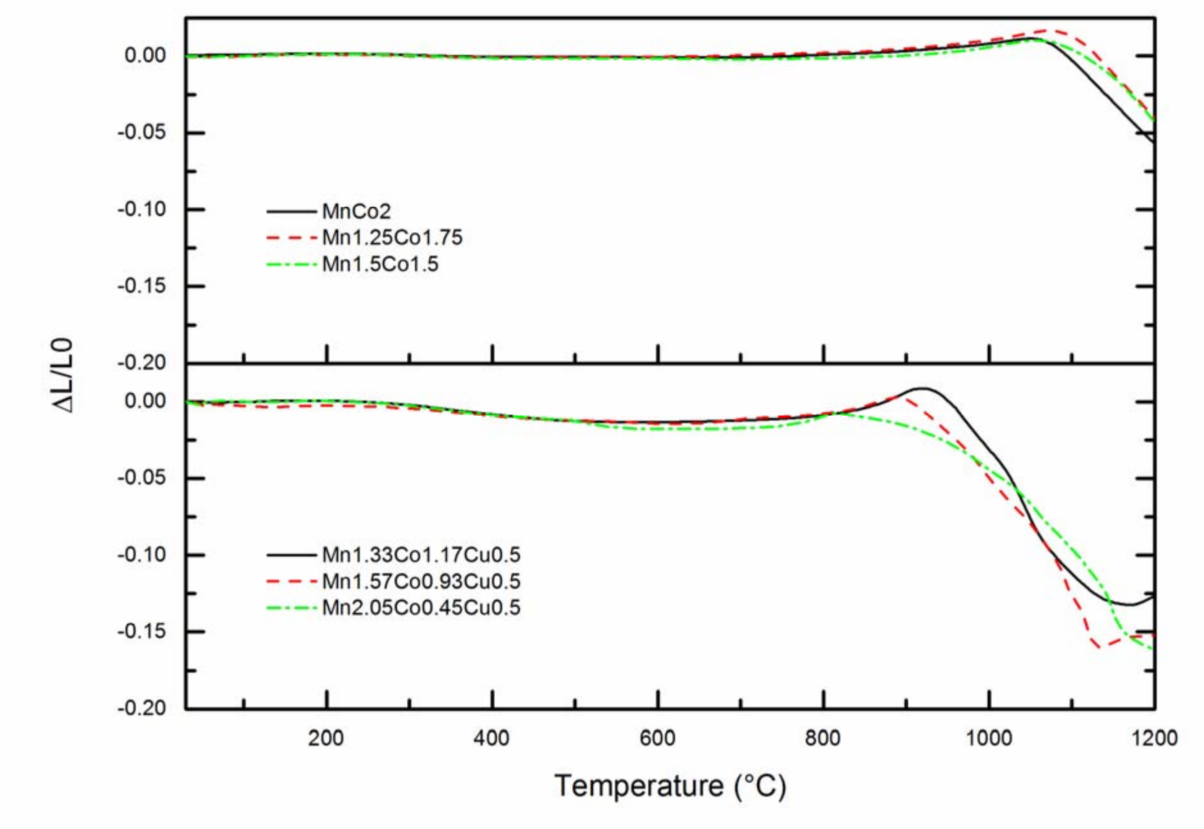

Fig. 4. Dilatometric curves as a function of temperature of the different samples.

The undesired phase segregation upon sintering at high temperature is an issue to precisely determine CTE and electrical properties of the material. Therefore, the sintering treatment of the pellets needed for dilatometry and Van der Pauw experiments was tailored. In the case of Mn-Co samples, it was not possible to reduce the temperature to avoid secondary phase formation, but a second dwell at lower temperature (i.e. 800°C) was successfully introduced to facilitate the spinel recovery. For MnCo2 sample a further annealing (16h at 1000°C) was required to achieve single phase pellets, as observed for similar samples prepared with other synthesis routes [8]. For Mn-Co-Cu samples instead, the lower sintering temperature setup, as observed in dilatometric measurements, allowed to reduce the thermal treatment to 1000°C, avoiding segregation of Cu-rich phases and still obtaining sufficiently dense pellets. In Fig. 5b-d SEM images of the Mn1.33Co1.17Cu0.5, Mn1.57Co0.93Cu0.5 and Mn2.05Co0.45Cu0.5 samples after sintering at 1000°C are reported. A homogeneous morphology can be observed, characterized by significantly lower crystal growth with respect to the 1200°C thermal treatment. In Table 3 a summary of the performed thermal treatments and the geometrical density measured after sintering is reported. It can be noted that Cu addition leads to densities comparable to Mn-Co samples even with a 200K reduction in sintering temperature.

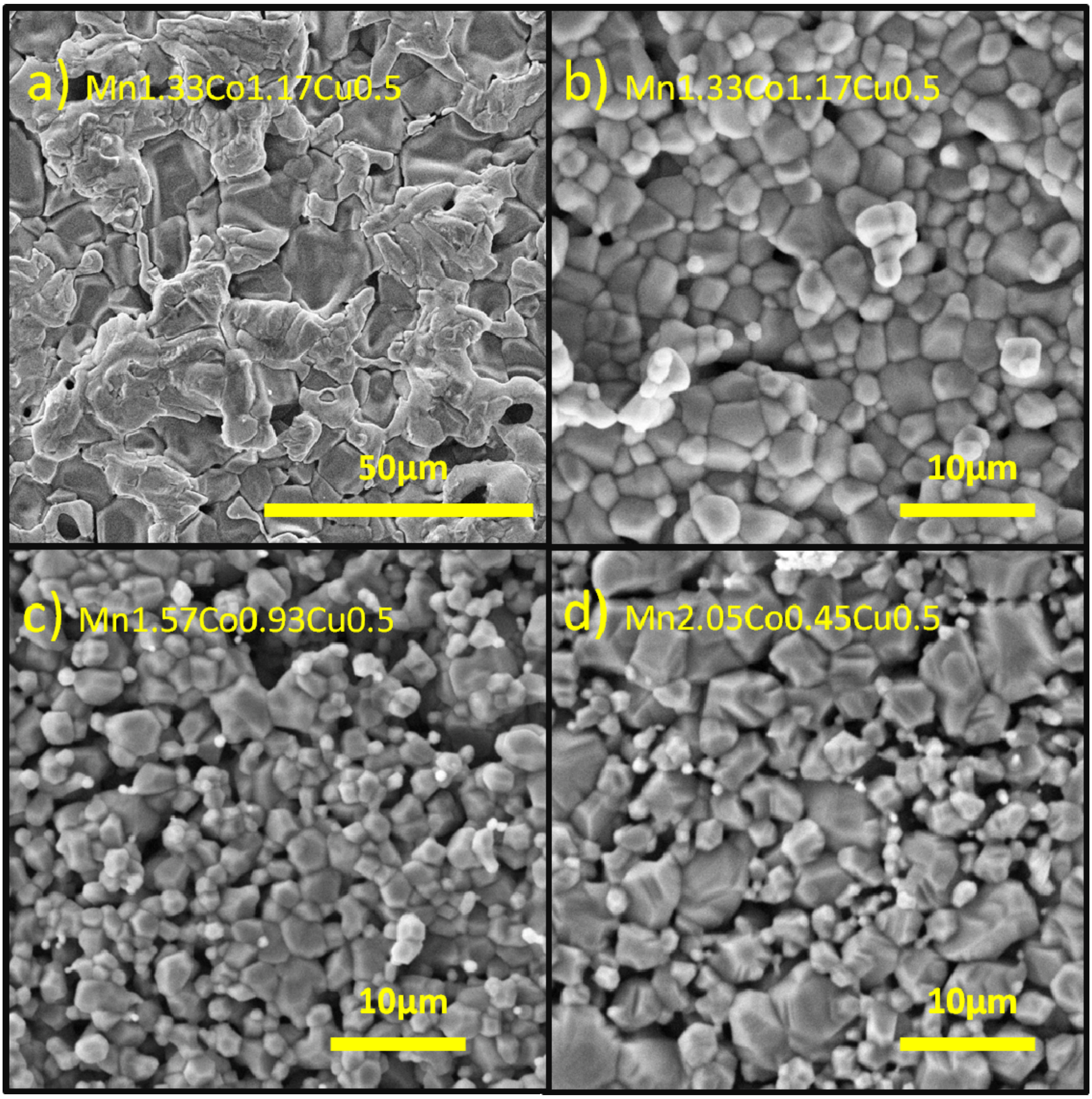

Fig. 5: SEM images of samples heat treated at a)1200°C and b,c,d) 1000°C (see text for details).

Table 3: Sintering thermal treatments:

Sample	Green density %	Sintering treatment	Sintered density %
MnCo2	66±1	4 h @1200°C + 4 h @800°C 16h @ 1000°C post sintering	93±1
Mn1.25Co1.75	67±1	4 h @1200°C + 4 h @800°C	93±1
Mn1.5Co1.5	67±1		95±2
Mn1.33Co1.17Cu0.5	65±1	4 h @1000°C + 4 h @800°C	97±1
Mn1.57Co0.93Cu0.5	64±1		97±2
Mn2.05Co0.45Cu0.5	65±1		97±2

In Fig. 6 X-Ray diffraction patterns of the sintered samples are reported. MnCo2 and Mn1.25Co1.75 show a pattern ascribable to a single cubic phase, with small shifts due to different Mn:Co ratio, while Mn1.5Co1.5 exhibits a mixture of a tetragonal and cubic spinels. These results are in agreement with the Mn-Co oxides phase diagram at room temperature. A single cubic phase is stable for high Co content (Co:Mn>1.3), a single tetragonal phase is obtained for high Mn content (Co:Mn<0.5), while for intermediate compositions, depending on the synthesis and cooling method, a mixture of the two phases or a single metastable tetragonal phase is observed[4,5]. Regarding Cu-Mn-Co samples, as observed by HT-XRD, Mn1.33Co1.17Cu0.5 is characterized by a single cubic phase, while raising Mn content peaks ascribable to a tetragonal spinel phase appear. Differently from Mn-Co composition, where Mn rich spinels exhibit a single tetragonal phase, copper addition enhances the cubic phase stability region, as evident by the phase composition of the Mn2.05Co0.45Cu0.5 sample, characterized by a mixture of cubic and tetragonal phases.

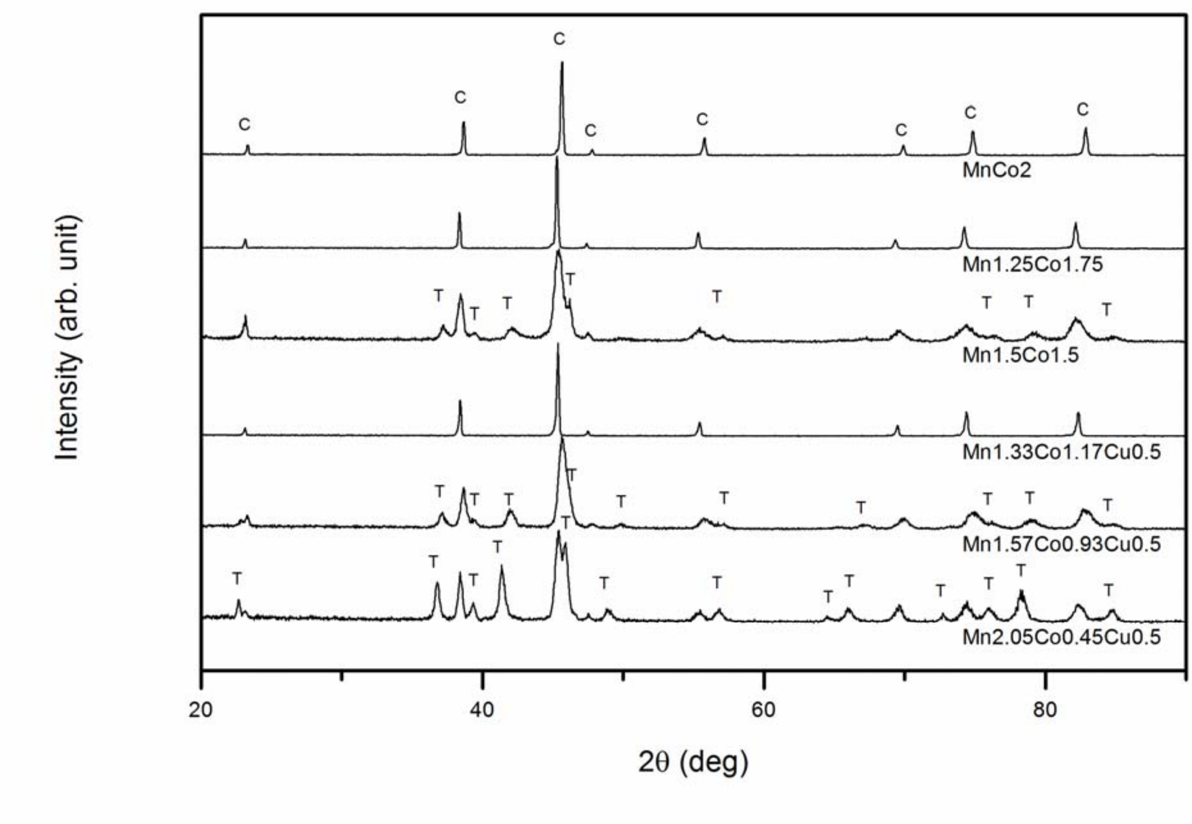

Fig. 6. X-ray powder diffraction patterns of the samples after sintering treatment; C specify reflections ascribable to a cubic spinel phase, T to a tetragonal spinel phase.

3.2. Thermal expansion

To evaluate the CTE of the different compositions, the sintered pellets were subjected to dilatometric analyses, and the obtained curves are reported in Fig. 7. Regarding Mn-Co samples, it can be observed that higher Co content induces higher expansion. MnCo2 and Mn1.25Co1.75 samples, characterized by a single phase in the whole examined temperature range, show a corresponding linear behaviour. Mn1.5Co1.5 curve shows instead a discontinuity in the 500-600°C temperature range, ascribable to the dual phase – single phase transition. Regarding copper addition, a similar behaviour can be observed: the dual-phase samples (those richest in Mn) exhibit a discontinuity in the 450-600°C temperature range and in the 600-750°C for the Mn1.57Co0.93Cu0.5 and Mn2.05Co0.45Cu0.5 samples respectively, most likely related to the dual-single phase transition occurring in these temperature intervals.

Average CTE values have been calculated between room temperature and 800°C, and are reported in Table 4. Among the considered composition, Mn1.57Co0.93Cu0.5 and Mn1.25Co1.75 exhibit the highest compatibility with thermal expansion of ferritic stainless steels ($11\text{-}13 \cdot 10^{-6}\ K^{-1}$ [28]). To evaluate how the different Mn:Co ratio and Cu addition influence CTE, in Fig. 8 are reported the CTE values at 800°C versus the cobalt content for the different samples. Regarding Mn-Co composition, a clear linear trend can be observed between the composition and CTE values. Also for Cu doped samples an analogue behaviour can be observed when changing Mn:Co ratio, and Cu addition does not affect significantly this trend but rather induces a shift of the curve toward higher CTEs.

The observed behaviour can be ascribed to the chemical differences between the samples considering lattice sites occupations and atoms valence. In particular, thermal expansion of mixed metal spinels can be related to the composition principally via the occupation of octahedral sites [29], where compounds characterized by high valence differences possess higher CTE.

Mn-Co spinels are characterized by a preferential occupation of tetrahedral sites by Co^{II} atoms. Co^{II}, Co^{III}, Mn^{III} and Mn^{IV} occupy octahedral sites, with Co^{II} and Mn^{IV} amounts related to electro-neutrality constraints [30]. In the $1{:}1 \leq Co{:}Mn \leq 2{:}1$ compositional range, the increase of Co promotes an increase of Co^{II}, Co^{III} and Mn^{IV} species at the expense of Mn^{III} atoms[31]. Increasing Co content in this composition range will cause therefore higher inhomogeneity, theoretically raising CTE, in agreement with our results.

In mixed Cu-Co-Mn compounds instead, Cu^{I}/Cu^{II} species tend to occupy tetrahedral sites preferentially over Co^{II} atoms, leading to an enrichment of Co^{II}/Co^{III} pairs in octahedral sites [32]. Furthermore, the presence of Cu^{I} atoms promotes Mn^{III} oxidation to Mn^{IV} to maintain charge neutrality. Valence differences are therefore increased with copper doping, enhancing CTE.

Table 4. Thermal expansion coefficient at 800°C measured for the different samples:

Sample	CTE @800°C ($\cdot 10^{-6}$ K^{-1})
MnCo2	13.5±0.1
Mn1.25Co1.75	11.5±0.1
Mn1.5Co1.5	9.7±0.1
Mn1.33Co1.17Cu0.5	14.5±0.1
Mn1.57Co0.93Cu0.5	12.7±0.1
Mn2.05Co0.45Cu0.5	8.5±0.1

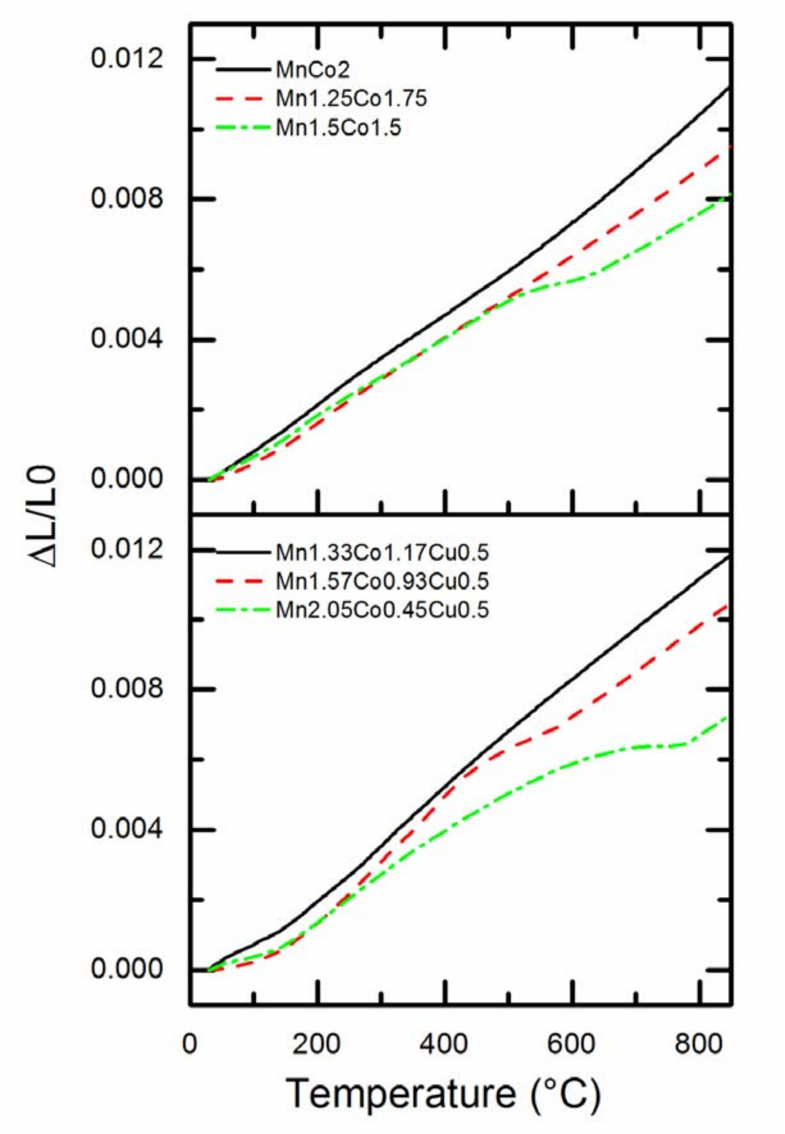

Fig. 7. Thermal expansion curves of the sintered samples.

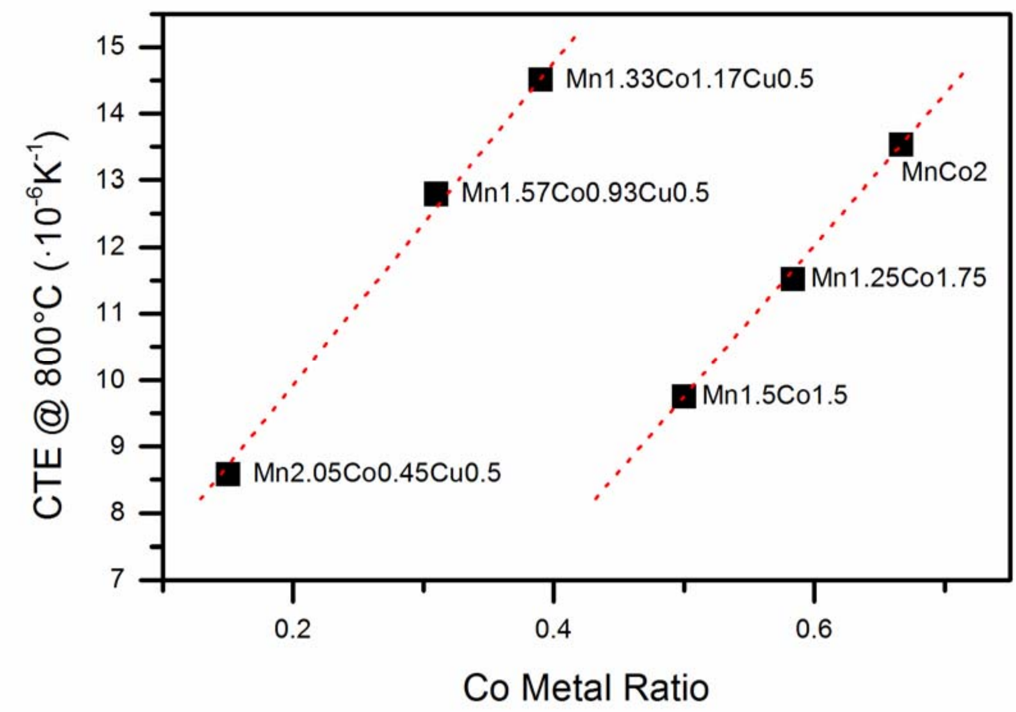

Fig. 8. Coefficient of thermal expansion calculated at 800°C as a function of the sample composition.

3.3. Electrical conductivity

Electrical conductivity measurement was carried out by means of the Van der Pauw method in the temperature range 500-800°C. In Fig. 9 are reported Arrhenius plots.

MnCo2, Mn1.25Co1.75 and Mn1.33Co1.17Cu0.5 samples exhibit a linear behaviour through all the examined range, as expected by their single phase nature. On the contrary, samples characterized by dual to single phase transitions show slope changes in their linear trend, at temperatures coherent with the discontinuities observed during dilatometric measurements. From the single-phase region of the Arrhenius plots, the activation energies were calculated and are reported in Table 5. Mn-Co samples exhibit comparable values of about 0.5eV, while Cu addition lowers significantly in all cases the activation energy to about 0.3eV.

To better evaluate how Mn:Co ratio and Cu addition affect electrical properties, in Fig. 10 are reported conductivity values measured at 800°C versus cobalt content. The MnCo2 sample is characterized by a conductivity value of about 80S/cm, and a decreasing trend can be observed increasing Mn content. A similar decrease in conductivity with Mn content can be observed for the Cu doped samples as well. On the other hand, Cu addition increases electrical conductivity, with the Mn1.33Co1.17Cu0.5 sample characterized by a conductivity value of about 125S/cm.

In such spinel systems, the conductivity behaviour is usually explained with a small polaron hopping mechanism between mixed valence elements on octahedral sites, and in Mn-Co oxides it is usually related to Co^{II}/Co^{III} and Mn^{III}/Mn^{IV} pairs [3,30,31]. The Co^{II}/Co^{III} and Mn^{III}/Mn^{IV} concentration ratio affects therefore conductivity properties, Co^{III} and Mn^{III} being the most common species in octahedral sites. The observed trend for Mn-Co samples is in agreement with previous findings, and is related to the maximum concentration of Co^{II} and Mn^{IV} species for compositions with Mn:Co≈2:1 [31]. The similar increasing trend here observed for the Cu-doped samples suggests that similar phenomena can be accounted for also in Cu-Mn-Co samples. The significant increase of conductivity in Cu samples with respect to Mn-Co compounds can be instead due to multiple mechanisms. Copper addition in mixed Mn-Co spinels occurs with preferential occupation of tetrahedral sites of the spinel lattice by Cu^{I} and Cu^{II} species, that promotes Mn^{III} oxidation to Mn^{IV} to maintain charge neutrality. As a consequence, Cu introduction increases active pairs concentration and therefore electrical conductivity [32]. Tetrahedral Cu ions could furthermore contribute indirectly to electrical conductivity, through mediation of charge transfer mechanisms between near but not adjacent Mn atoms, as observed in Ni-Cu manganite spinels [33].

Table 5. Activation energy calculated from the Arrhenius plot of 10 hours milled samples:

Sample	Temperature range (°C)	Ea (eV)
MnCo2	500-800	0.55±0.02
Mn1.25Co1.75	500-800	0.54±0.04

Mn1.5Co1.5	650-800	0.49±0.02
Mn1.33Co1.17Cu0.5	500-800	0.34±0.02
Mn1.57Co0.93Cu0.5	600-800	0.32±0.03
Mn2.05Co0.45Cu0.5	750-800	0.32±0.04

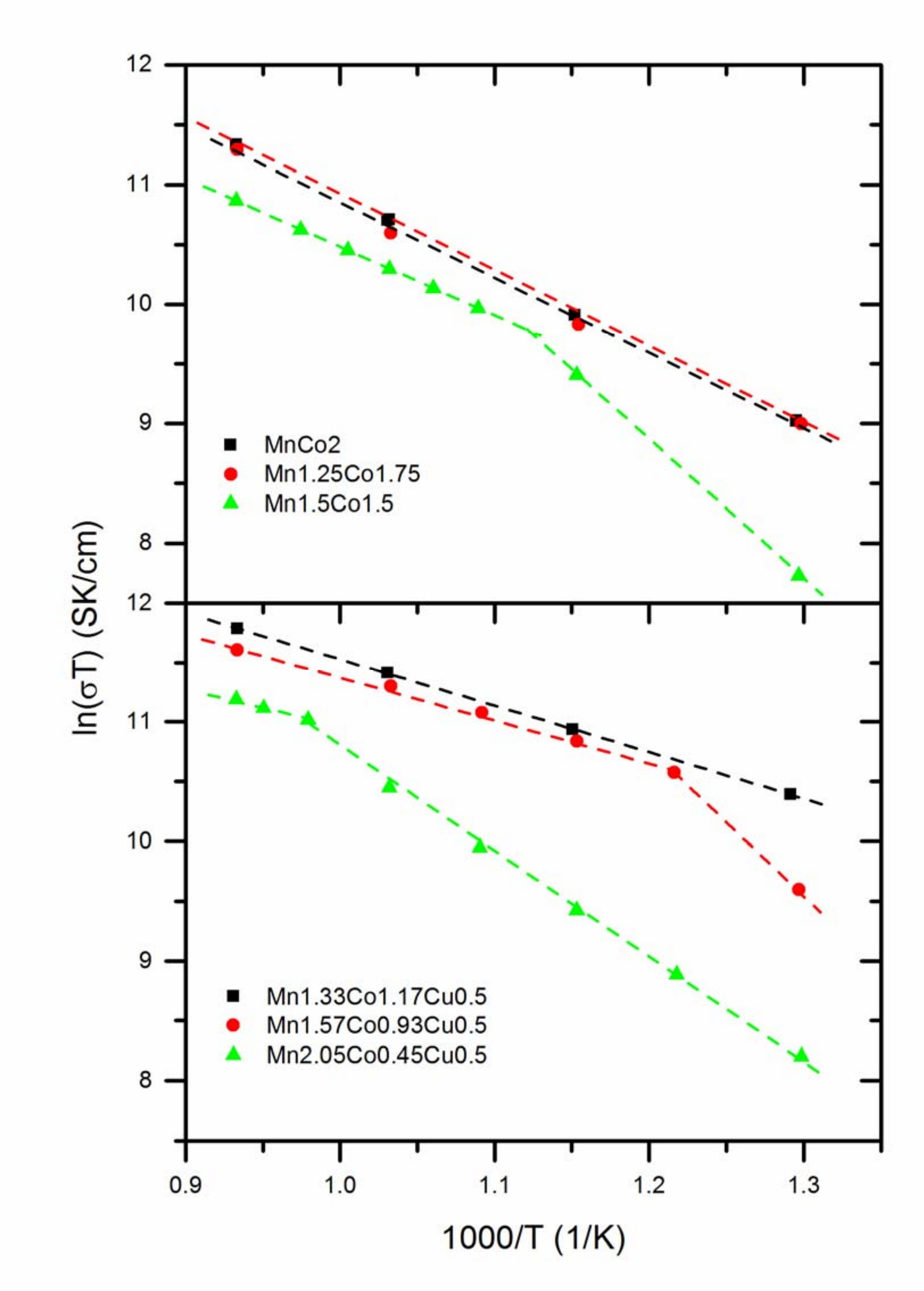

387

388 *Fig. 9: Arrhenius plots of electrical conductivity measured for the different samples.*

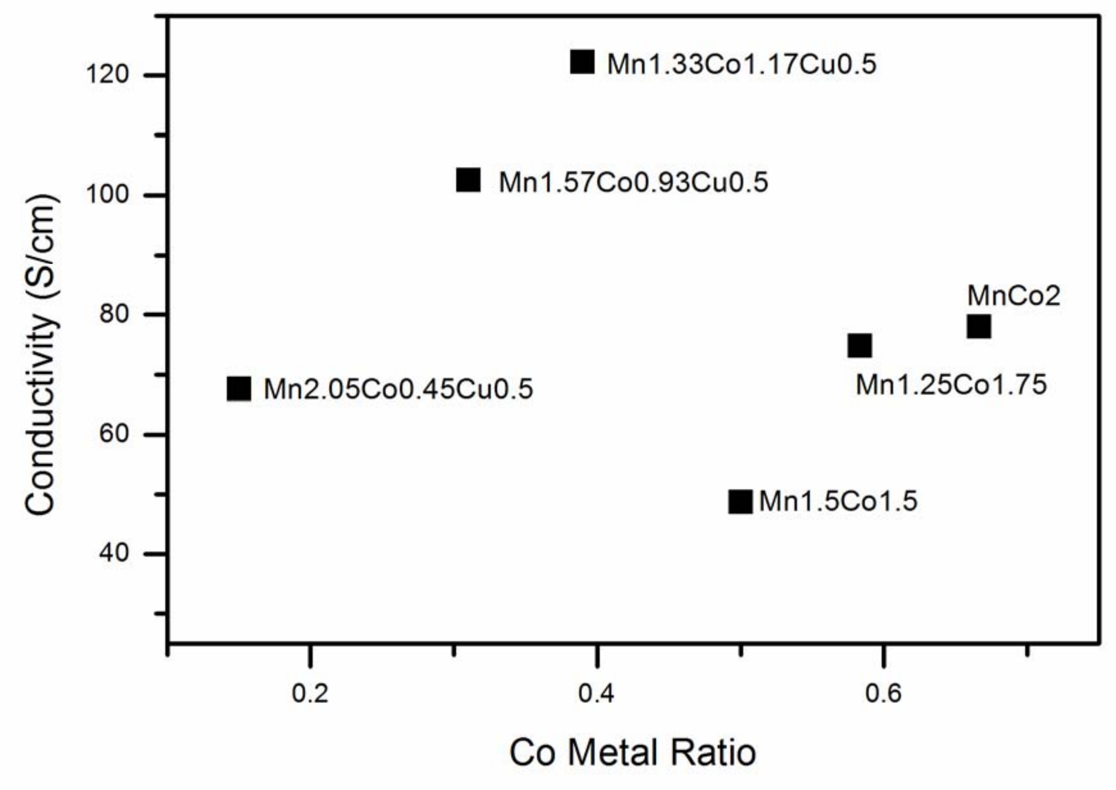

Fig. 10. Conductivity values measured at 800°C as a function of the sample composition.

4. Conclusions

Different Mn-Co and Cu-Mn-Co spinels were synthesised in order to evaluate the effect of Mn:Co ratio and copper addition on sintering behaviour, thermal expansion and electrical conductivity.

A High Energy Ball Milling treatment of oxide powders was utilized to produce highly reactive metastable multi-phase compounds that easily homogenize when brought to intermediate temperature (T<800°C) to form the equilibrium products. The influence of the different spinel compositions was observed on high temperature (T>1000°C) behaviour of each compound, evidencing that Cu decreases the spinel stability region. Thermogravimetric and in situ high temperature XRD analysis allowed to observe for the examined Cu-Mn-Co compositions a single cubic phase stable at high operating temperature (800°C). Different Mn:Co ratios did not lead to significant differences in sintering behaviour, while Copper addition proved to be highly effective in reducing sintering temperature and obtaining high densities.

Dilatometry experiments performed on sintered pellets allowed to observe a simple relation between CTE and composition: CTE similarly increases with cobalt content, both in Mn-Co and Cu-Mn-Co samples, with Cu doped samples characterized by higher CTE values.. A similar relation could be observed also from electrical conductivity, being enhanced (up to 125S/cm) by Cu addition and high cobalt content. The thermal expansion and electrical conductivity of Mn-Co spinels can thus be tuned by varying stoichiometry.

Despite the best coating spinel composition cannot be given in absolute, because depending on the interconnector alloy (and its CTE) and on the deposition process used, it is possible to state that the fine tuning of stoichiometry is the strategy to design an ideal coating spinel. Cu addition to spinels characterized by the opportune Mn-Co ratio represent a further possibility to optimize a material capable to satisfy the properties required by the interconnect coating with the advantage of limiting the use of an expensive and toxic element like Co.

Acknowledgments

This work is supported by the FCH JU within the project SCORED 2:0 under contract. 325331. The authors wish to thank Dr. Claudia Paoletti for the technical support and useful discussions.

Bibliography

[1] N. Shaigan, W. Qu, D.G. Ivey, W. Chen, A review of recent progress in coatings, surface modifications and alloy developments for solid oxide fuel cell ferritic stainless steel interconnects, J. Power Sources. 195 (2010) 1529–1542. doi:10.1016/j.jpowsour.2009.09.069.

[2] J. Wu, X. Liu, Recent development of SOFC metallic interconnect, J. Mater. Sci. Technol. 26 (2010) 293–305. doi:10.1016/S1005-0302(10)60049-7.

[3] A. Petric, H. Ling, Electrical Conductivity and Thermal Expansion of Spinels at Elevated Temperatures, J. Am. Ceram. Soc. 90 (2007) 1515–1520. doi:10.1111/j.1551-2916.2007.01522.x.

[4] E. Aukrust, A. Muan, Phase Relations in the System Cobalt Oxide-Manganese Oxide in Air, J. Am. Ceram. Soc. 46 (1963) 511–511. doi:10.1111/j.1151-2916.1963.tb13790.x.

[5] Y.V. Golikov, S.Y. Tubin, V.P. Barkhatov, V.F. Balakirev, Phase diagrams of the Co-Mn-O system in air, J. Phys. Chem. Solids. 46 (1985) 539–544. doi:10.1016/0022-3697(85)90215-X.

[6] X. Xin, S. Wang, Q. Zhu, Y. Xu, T. Wen, A high performance nano-structure conductive coating on a Crofer22APU alloy fabricated by a novel spinel powder reduction coating technique, Electrochem. Commun. 12 (2010) 40–43. doi:10.1016/j.elecom.2009.10.031.

[7] Y. Xu, Z. Wen, S. Wang, T. Wen, Cu doped Mn–Co spinel protective coating on ferritic stainless steels for SOFC interconnect applications, Solid State Ionics. 192 (2011) 561–564. doi:10.1016/j.ssi.2010.05.052.

[8] Y. Liu, J.W. Fergus, K. Wang, C. Dela Cruz, Crystal Structure, Chemical Stabilities and Electrical Conductivity of Fe-Doped Manganese Cobalt Spinel Oxides for SOFC Interconnect Coatings, J. Electrochem. Soc. 160 (2013) F1316–F1321.

doi:10.1149/2.114311jes.

[9] B.-K. Park, J.-W. Lee, S.-B. Lee, T.-H. Lim, S.-J. Park, C.-O. Park, R.-H. Song, Cu- and Ni-doped Mn1.5Co1.5O4 spinel coatings on metallic interconnects for solid oxide fuel cells, Int. J. Hydrogen Energy. 38 (2013) 12043–12050. doi:10.1016/j.ijhydene.2013.07.025.

[10] Z. Yang, G. Xia, S.P. Simner, J.W. Stevenson, Thermal Growth and Performance of Manganese Cobaltite Spinel Protection Layers on Ferritic Stainless Steel SOFC Interconnects, J. Electrochem. Soc. 152 (2005) A1896. doi:10.1149/1.1990462.

[11] Z. Yang, G.-G. Xia, X.-H. Li, J.W. Stevenson, (Mn,Co)3O4 spinel coatings on ferritic stainless steels for SOFC interconnect applications, Int. J. Hydrogen Energy. 32 (2007) 3648–3654. doi:10.1016/j.ijhydene.2006.08.048.

[12] K. Wang, Y. Liu, J.W. Fergus, Interactions Between SOFC Interconnect Coating Materials and Chromia, J. Am. Ceram. Soc. 94 (2011) 4490–4495. doi:10.1111/j.1551-2916.2011.04749.x.

[13] M.Y. Yoon, E.J. Lee, R.H. Song, H.J. Hwang, Preparation and properties of a MnCo2O4 for ceramic interconnect of solid oxide fuel cell via glycine nitrate process, Met. Mater. Int. 17 (2011) 1039–1043. doi:10.1007/s12540-011-6025-5.

[14] Y. Liu, J.W. Fergus, C. Dela Cruz, Electrical properties, cation distributions, and thermal expansion of manganese cobalt chromite spinel oxides, J. Am. Ceram. Soc. 96 (2013) 1841–1846. doi:10.1111/jace.12254.

[15] G. Chen, X. Xin, T. Luo, L. Liu, Y. Zhou, C. Yuan, C. Lin, Z. Zhan, S. Wang, Mn1.4Co1.4Cu0.2O4 spinel protective coating on ferritic stainless steels for solid oxide fuel cell interconnect applications, J. Power Sources. 278 (2015) 230–234. doi:10.1016/j.jpowsour.2014.12.070.

[16] J. Xiao, W. Zhang, C. Xiong, B. Chi, J. Pu, L. Jian, Oxidation of MnCu0.5Co1.5O4 spinel

coated SUS430 alloy interconnect in anode and cathode atmospheres for intermediate temperature solid oxide fuel cell, Int. J. Hydrogen Energy. 40 (2015) 1868–1876. doi:10.1016/j.ijhydene.2014.11.124.

[17] A. Masi, M. Bellusci, M. Carlini, S.J. McPhail, F. Padella, P. Reale, Mechanochemical Processing of Mn and Co Oxides: An Alternative Way to Synthesize Mixed Spinels for Protective Coating, J. Am. Ceram. Soc. 99 (2016) 308–314. doi:10.1111/jace.13863.

[18] P. Baláž, M. Achimovičová, M. Baláž, P. Billik, Z. Cherkezova-Zheleva, J.M. Criado, F. Delogu, E. Dutková, E. Gaffet, F.J. Gotor, R. Kumar, I. Mitov, T. Rojac, M. Senna, A. Streletskii, K. Wieczorek-Ciurowa, Hallmarks of mechanochemistry: from nanoparticles to technology, Chem. Soc. Rev. 42 (2013) 7571. doi:10.1039/c3cs35468g.

[19] F. Delogu, L. Schiffini, G. Cocco, The invariant laws of the amorphization processes by mechanical alloying, Philos. Mag. A. 81 (2001) 1917–1937. doi:10.1080/01418610010019107.

[20] A. Boschetto, M. Bellusci, A. La Barbera, F. Padella, F. Veniali, Kinematic observations and energy modeling of a Zoz Simoloyer high-energy ball milling device, Int. J. Adv. Manuf. Technol. 69 (2013) 2423–2435. doi:10.1007/s00170-013-5201-9.

[21] N. Burgio, A. Iasonna, M. Magini, S. Martelli, F. Padella, Mechanical alloying of the Fe−Zr system. Correlation between input energy and end products, Nuovo Cim. D. 13 (1991) 459–476. doi:10.1007/BF02452130.

[22] ICPDS.ICDD, -, PCPDF-WIN Version 2.01. (1998).

[23] S. Brunauer, P.H. Emmett, E. Teller, Adsorption of Gases in Multimolecular Layers, J. Am. Chem. Soc. 60 (1938) 309–319. doi:10.1021/ja01269a023.

[24] L.J. van der Pauw, A method of measuring the resistivity and Hall coefficient on lamellae of arbitrary shape, Philips Tech. Rev. 20 (1958) 220–224.

[25] G.C. Wood, T. Hodgkiess, The Hardness of Oxides at Ambient Temperatures, Mater. Corros. Und Korrosion. 23 (1972) 766–773. doi:10.1002/maco.19720230905.

[26] B. Gillot, DTG Curves of Selective Oxidation of Submicrometer Mixed Valency Spinels: Data Table for the Oxidation Temperature of Transition Metals and Its Relation to the Cation-Oxygen Distance, J. Solid State Chem. 113 (1994) 163–167. doi:10.1006/jssc.1994.1355.

[27] R.M. German, P. Suri, S.J. Park, Review: Liquid phase sintering, J. Mater. Sci. 44 (2009) 1–39. doi:10.1007/s10853-008-3008-0.

[28] Z. Yang, K.S. Weil, D.M. Paxton, J.W. Stevenson, Selection and Evaluation of Heat-Resistant Alloys for SOFC Interconnect Applications, J. Electrochem. Soc. 150 (2003) A1188. doi:10.1149/1.1595659.

[29] G. Bayer, Thermal expansion of oxide compounds with spinel structure, Thermochim. Acta. 3 (1972) 421–426. doi:10.1016/0040-6031(72)85001-9.

[30] H. Bordeneuve, A. Rousset, C. Tenailleau, S. Guillemet-Fritsch, Cation distribution in manganese cobaltite spinels Co3−x Mn x O4 ($0 \leq x \leq 1$) determined by thermal analysis, J. Therm. Anal. Calorim. 101 (2010) 137–142. doi:10.1007/s10973-009-0557-7.

[31] H. Bordeneuve, C. Tenailleau, S. Guillemet-Fritsch, R. Smith, E. Suard, A. Rousset, Structural variations and cation distributions in Mn3−xCoxO4 ($0 \leq x \leq 3$) dense ceramics using neutron diffraction data, Solid State Sci. 12 (2010) 379–386. doi:10.1016/j.solidstatesciences.2009.11.018.

[32] P. a. Wright, S. Natarajan, J.M. Thomas, P.L. Gai-Boyes, Mixed-metal amorphous and spinel phase oxidation catalysts: characterization by x-ray diffraction, x-ray absorption, electron microscopy, and catalytic studies of systems containing copper, cobalt, and manganese, Chem. Mater. 4 (1992) 1053–1065. doi:10.1021/cm00023a024.

[33] E. Elbadraoui, Cation distribution and mechanism of electrical conduction in nickel-copper manganite spinels, Solid State Ionics. 93 (1997) 219–225. doi:10.1016/S0167-2738(96)00559-0.